

1 **SUPPLEMENTARY INFORMATION**

2 **The increasing atmospheric burden of the greenhouse gas sulfur hexafluoride (SF₆)**

3
4
5 Peter G. Simmonds¹, Matthew Rigby¹, Alistair J. Manning⁴, Sunyoung Park⁸, Kieran M.
6 Stanley^{1,10}, Archie McCulloch¹, Stephan Henne², Francesco Graziosi¹¹, Michela Maione¹¹,
7 Jgor Arduini¹¹, Stefan Reimann², Martin K. Vollmer², Jens Mühle³, Simon O'Doherty¹, Dickon
8 Young¹, Paul B. Krummel⁵, Paul J. Fraser⁵, Ray F. Weiss³, Peter K. Salameh³, Christina M.
9 Harth³, Mi-Kyung Park⁹, Hyeri Park⁹, Tim Arnold^{12,13}, Chris Rennick¹², L. Paul Steele⁵,
10 Blagoj.Mitrevski⁵, Ray H. J. Wang⁶, and Ronald G. Prinn⁷.

11

12 ¹ School of Chemistry, University of Bristol, Bristol, UK.

13 ² Swiss Federal Laboratories for Materials Science and Technology, Laboratory for Air
14 Pollution and Environmental Technology (Empa), Dübendorf, Switzerland.

15 ³ Scripps Institution of Oceanography (SIO), University of California, San Diego, La Jolla,
16 California, USA.

17 ⁴ Met Office Hadley Centre, Exeter, UK.

18 ⁵ Climate Science Centre, Commonwealth Scientific and Industrial Research Organisation
19 (CSIRO), Oceans and Atmosphere, Aspendale, Victoria, Australia.

20 ⁶ School of Earth, and Atmospheric Sciences, Georgia Institute of Technology, Atlanta,
21 Georgia, USA.

22 ⁷ Center for Global Change Science, Massachusetts Institute of Technology, Cambridge,
23 Massachusetts, USA.

24 ⁸ Department of Oceanography, Kyungpook National University, Daegu, Republic of Korea.

25 ⁹ Kyungpook Institute of Oceanography, Kyungpook National University, Daegu, Republic of
26 Korea.

27 ¹⁰ Institute for Atmospheric and Environmental Sciences, Goethe University Frankfurt,
28 Germany.

29 ¹¹ Department of Pure and Applied Sciences (DISPEA) of the University of Urbino and
30 Institute of Atmospheric Sciences and Climate (ISAC) of the National Research Council
31 (CNR), Bologna, Italy.

32 ¹²National Physical Laboratory, Teddington, United Kingdom.

33 ¹³School of GeoSciences, University of Edinburgh, Edinburgh, UK.

34

35 Correspondence to: P.G. Simmonds (petergsimmonds@aol.com)

36

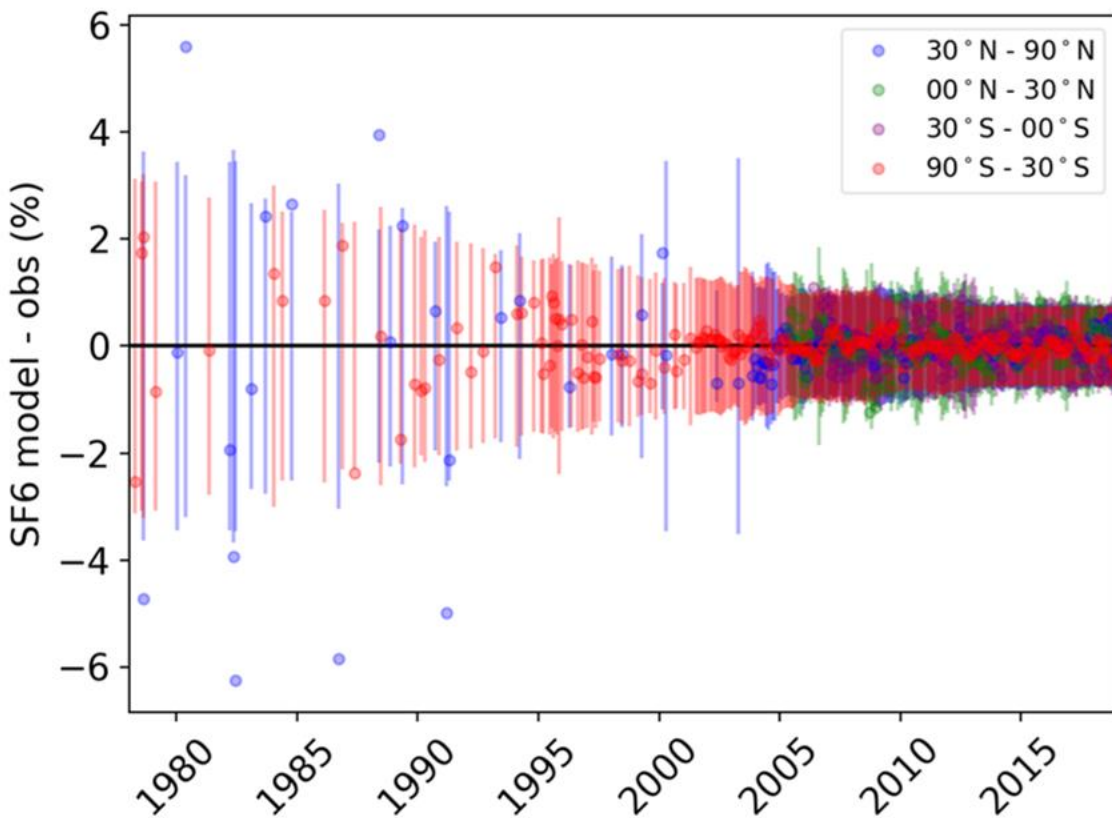
37

38

39

40

41 In this supplementary information we include:-
42
43 Figure S1. SF₆ model/measurement comparison from the AGAGE 12-box model.
44 A detailed description of the InTEM and EBRIS inversion models used to estimate regional
45 emissions.
46 Table S1. InTEM Meteorology.
47 Table S2. Rand Corporation sales of SF₆ to End-Use applications.
48 Table S3. InTEM emissions estimates for South Korea.
49



50
51 Figure S1. SF₆ model/measurement comparison from the AGAGE 12-box model.
52

53 InTEM model description

54 InTEM is a Bayesian system that minimises the mismatch between the model and the
55 atmospheric observations given the constraints imposed by the observation and model
56 uncertainties and prior information with its associated uncertainties. The horizontal and vertical
57 resolution of the meteorology has improved over the modelled period and is described in Table
58 ST1. The direction (latitude and longitude) and altitude varying background concentration and
59 observation station bias are solved for within the inverse system along with the spatial
60 distribution and magnitude of the emissions. The time-varying prior background concentration
61 for the DECC network stations is derived from the MHD observations when they are very
62 largely sensitive only to Northern Canada (Arnold et al., 2018), JFJ and CMN prior baselines

63 are derived separately for each station using times when the land influence at these high altitude
 64 stations is small. The prior bias (that can be positive or negative) for each station is set to zero
 65 with an uncertainty of 0.02 ppt. The population-weighted prior has a total domain uncertainty
 66 of 200% and has a domain-wide emission of 2 Gg yr⁻¹. The observations from each station are
 67 assumed to have an exponentially decreasing 12-hr time correlation coefficient and, between
 68 stations, a 200 km spatial correlation coefficient. The observations are averaged into 2-hr
 69 periods. The uncertainty of the observations is derived from the reported daily observation
 70 precision uncertainty and the variability of the observations within a 6-hr period. The modelling
 71 uncertainty for each 2-hr period at each station varies and is defined as the larger of; the median
 72 pollution event in that year at that station, or 16.5% of the magnitude of the pollution event.
 73 These values have been derived from analysis of the observations of methane at multiple
 74 heights at each station across the DECC network. Each inversion (2-month with 7-sites, 2-yr
 75 with 3-sites or 3-yr when only MHD is available) is repeated 24 times, each time 10% of the
 76 observations per year per station are randomly removed in 5-day intervals and the results and
 77 uncertainty averaged. This random removal of observations allows a greater exploration of the
 78 uncertainty, given the potential for some of the emission sources to be intermittent within the
 79 time-period of the inversion.

80

81 **TABLE ST1. 3-DIMENSIONAL METEOROLOGY USED TO DRIVE NAME FOR DIFFERENT**
 82 **YEARS. FOR DECC OBSERVATIONS FROM 2012 ONWARDS THE HIGH RESOLUTION UM**
 83 **METEOROLOGY (LAST LINE) CALCULATED OVER THE UK IS USED NESTED INSIDE THE**
 84 **GLOBAL METEOROLOGY DATA.**

Year	Horizontal Resolution	Number Levels	Vertical	Time Resolution
Aug 2002 – Dec 2005	~60 km	32		
Dec 2005 – Mar 2011	~40km	32	3hr	
Mar 2011 – Jul 2014	~25 km	53	3hr	
Jul 2014 – Jul 2017	~17 km	53	3hr	
Jul 2017 – Dec 2018	~12 km	53	3hr	
Jan 2012 – Dec 2018 (MHD and TAC only)	~ 1.5 km	58		1hr

85

86 Arnold, T., Manning, A. J., Kim, J., Li, S., Webster, H., Thomson, D., Mühle, J., Weiss, R.
 87 F., Park, S., and O'Doherty, S.: Inverse modelling of CF₄ and NF₃ emissions in East Asia,
 88 Atmos. Chem. Phys., 18, 13305-13320, 10.5194/acp-18-13305-2018, 2018.
 89 Cullen, M. J. P.: The unified forecast/climate model, Meteorol. Mag., 122, 81–94, 1993.
 90 Jones, A., Thomson, D., Hort, M., and Devenish, B.: The UK Met Office's next-generation
 91 atmospheric dispersion model, NAME III, Air Pollution Modeling and Its Applications XVII,
 92 edited by: Borrego, C. and Norman, A. L., 580–589, 2007.

93

94

95 **Definite Empa Bayesian Regional Inversion System (EBRIS)**

96
97 Surface source sensitivities used by the Empa inverse modelling system were derived with
98 the Lagrangian Particle Dispersion Model (LPDM) FLEXPART (Version 9.1, Stohl et al.,
99 2005) driven by analysis/forecasts from the operational runs of the Integrated Forecast Systems
100 (IFS) of the European Centre for Medium-Range Weather Forecasts (ECMWF). The horizontal
101 resolution of the input data was $0.2^\circ \times 0.2^\circ$ over the larger Alpine area and $1^\circ \times 1^\circ$ elsewhere. For
102 each observation site 3-hourly release intervals using 50'000 model particles each were
103 defined. These particles were traced backward in time for 10 days. Residence times of the
104 model particles within a regular geographic grid covering Europe and North America and
105 below a sampling height of 100 m were evaluated to derive the source sensitivities.

106 The regional scale inversion method applied by Empa was described in detail by Henne et
107 al. (2016), where it was applied to CH₄ emissions in Switzerland. The system was applied to
108 various halocarbon emission estimations in Europe (Brunner et al., 2017; Schoenenberger et
109 al., 2018) and East Asia (Vollmer et al., 2018; Lunt et al., 2018; Rigby et al., 2019). The method
110 follows a Bayesian approach in that it optimises the spatiotemporal emission distribution so
111 that simulation and observation of atmospheric concentrations best agree under the restriction
112 of a given a priori emission distribution and its uncertainties. The inversion grid contains
113 variable grid resolution following the average simulated source sensitivity with smaller (larger)
114 grid cells at location with larger (smaller) source sensitivities. The total simulated concentration
115 is separated into the regional contribution covered by the transport model and a baseline
116 fraction. Here, the baseline was estimated from the observed time series at each site separately
117 using the method by Ruckstuhl et al. (2012). The resulting baselines were included as part of
118 the state vector using linear interpolation for times between 5-daily baseline nodes.

119 The inversion was applied to yearly batches of observations solving for mean annual
120 emissions for the period 2007 to 2016. All valid observations from all sites were used in the
121 inverse estimate. We did not apply any additional filtering of the observations by time-of-day,
122 wind speed or direction. We followed the approach by Stohl et al. (2009) to avoid negative a
123 posteriori emissions in individual grid cells. A priori emissions for SF₆ were set to 0.46 Gg yr⁻¹
124 for the whole inversion domain, which covered Western and Central Europe. Emissions were
125 spatially disaggregated proportionally to population densities (Center for International Earth
126 Science Information Network, 2016). A-priori emissions were kept the same for all years. The
127 structure and the values of the covariance matrices for the a priori and data-mismatch
128 uncertainties were described by a set of parameters characterising absolute uncertainty levels
129 and spatiotemporal correlations in the uncertainties (Henne et al., 2016). These parameters
130 included the treatment of autocorrelation in the observations with a temporal correlation length
131 of 0.25 days. A maximum likelihood approach to obtain the uncertainty parameters as used
132 previously (Henne et al., 2016) did not converge for the current set of inversions. Therefore,
133 these parameters were set based on expert judgment and using an iterative approach to
134 determine the data-mismatch uncertainty (Stohl et al., 2009). The uncertainty of the a priori
135 emissions for the entire inversion domain was set to 100 %. The spatial correlation length scale
136 of the a priori was fixed to a value of 200 km. The uncertainty of the baseline was taken from
137 the fit to the observations (36 ppt, 41 ppt, 80 ppt and 128 ppt for the sites MHD, TAC, JFJ and
138 CMN). A common correlation length scale for the baseline of 30 days was assumed.

139

140 Brunner, D., T. Arnold, S. Henne, A. Manning, R. L. Thompson, M. Maione, S. O'Doherty,
141 and S. Reimann, 2017: Comparison of four inverse modelling systems applied to the

142 estimation of HFC-125, HFC-134a, and SF₆ emissions over Europe. *Atmos. Chem. Phys.*, **17**,
143 10651-10674, doi: 10.5194/acp-17-10651-2017.

144 Center for International Earth Science Information Network, C. C. U.: Gridded Population of
145 the World, Version 4 (GPWv4): Population Density Adjusted to Match 2015 Revision UN
146 WPP Country Totals. [Available online from <http://dx.doi.org/10.7927/H4HX19NJ>.]

147 Henne, S., D. Brunner, B. Oney, M. Leuenberger, W. Eugster, I. Bamberger, F. Meinhardt,
148 M. Steinbacher, and L. Emmenegger, 2016: Validation of the Swiss methane emission
149 inventory by atmospheric observations and inverse modelling. *Atmos. Chem. Phys.*, **16**, 3683-
150 3710, doi: 10.5194/acp-16-3683-2016.

151 Lunt, M. F., S. Park, S. Li, S. Henne, A. J. Manning, A. L. Ganesan, I. J. Simpson, D. R.
152 Blake, Q. Liang, S. O'Doherty, C. M. Harth, J. Muhle, P. K. Salameh, R. F. Weiss, P. B.
153 Krummel, P. J. Fraser, R. G. Prinn, S. Reimann, and M. Rigby, 2018: Continued Emissions
154 of the Ozone-Depleting Substance Carbon Tetrachloride From Eastern Asia. *Geophys. Res.
155 Lett.*, **45**, 11423-11430, doi: 10.1029/2018GL079500.

156 Rigby, M., S. Park, T. Saito, L. M. Western, A. L. Redington, X. Fang, S. Henne, A. J.
157 Manning, R. G. Prinn, G. S. Dutton, P. J. Fraser, A. L. Ganesan, B. D. Hall, C. M. Harth, J.
158 Kim, K. R. Kim, P. B. Krummel, T. Lee, S. Li, Q. Liang, M. F. Lunt, S. A. Montzka, J.
159 Muhle, S. O'Doherty, M. K. Park, S. Reimann, P. K. Salameh, P. Simmonds, R. L.
160 Tunnicliffe, R. F. Weiss, Y. Yokouchi, and D. Young, 2019: Increase in CFC-11 emissions
161 from eastern China based on atmospheric observations. *Nature*, **569**, 546-550, doi:
162 10.1038/s41586-019-1193-4.

163 Ruckstuhl, A. F., S. Henne, S. Reimann, M. Steinbacher, M. K. Vollmer, S. O'Doherty, B.
164 Buchmann, and C. Hueglin, 2012: Robust extraction of baseline signal of atmospheric trace
165 species using local regression. *Atmos. Meas. Tech.*, **5**, 2613-2624, doi: 10.5194/amt-5-2613-
166 2012.

167 Schoenenberger, F., S. Henne, M. Hill, M. K. Vollmer, G. Kouvarakis, N. Mihalopoulos, S.
168 O'Doherty, M. Maione, L. Emmenegger, T. Peter, and S. Reimann, 2018: Abundance and
169 sources of atmospheric halocarbons in the Eastern Mediterranean. *Atmos. Chem. Phys.*, **18**,
170 4069-4092, doi: 10.5194/acp-18-4069-2018.

171 Stohl, A., C. Forster, A. Frank, P. Seibert, and G. Wotawa, 2005: Technical note: The
172 Lagrangian particle dispersion model FLEXPART version 6.2. *Atmos. Chem. Phys.*, **5**, 2461-
173 2474, doi: 10.5194/acp-5-2461-2005.

174 Stohl, A., P. Seibert, J. Arduini, S. Eckhardt, P. Fraser, B. R. Greally, C. Lunder, M. Maione,
175 J. Mühle, S. O'Doherty, R. G. Prinn, S. Reimann, T. Saito, N. Schmidbauer, P. G. Simmonds,
176 M. K. Vollmer, R. F. Weiss, and Y. Yokouchi, 2009: An analytical inversion method for
177 determining regional and global emissions of greenhouse gases: Sensitivity studies and
178 application to halocarbons. *Atmos. Chem. Phys.*, **9**, 1597-1620, doi: 10.5194/acp-9-1597-
179 2009.

180 Vollmer, M. K., D. Young, C. M. Trudinger, J. Mühle, S. Henne, M. Rigby, S. Park, S. Li,
181 M. Guillevic, B. Mitrevski, C. M. Harth, B. R. Miller, S. Reimann, B. Yao, L. P. Steele, S. A.
182 Wyss, C. R. Lunder, J. Arduini, A. McCulloch, S. Wu, T. S. Rhee, R. H. J. Wang, P. K.
183 Salameh, O. Hermansen, M. Hill, R. L. Langenfelds, D. Ivy, S. O'Doherty, P. B. Krummel,
184 M. Maione, D. M. Etheridge, L. Zhou, P. J. Fraser, R. G. Prinn, R. F. Weiss, and P. G.
185 Simmonds, 2018: Atmospheric histories and emissions of chlorofluorocarbons CFC-13
186 (CClF₃), CFC-114 (C₂Cl₂F₄), and CFC-115 (C₂ClF₅). *Atmos. Chem. Phys.*, **18**, 979-1002, doi:
187 10.5194/acp-18-979-2018.

188

189 Table S2. Rand Corporation Sales of SF₆ to End-Use applications.

	Utilities (Gg)	Equipment (Gg)	*Magnesium (Gg)	*Electronics (Gg)	Adiabatic (Gg)	*Other Uses (Gg)	*Combined Prompt Emissions (Gg)
1996	1.136	4.770	0.530	0.303	0.379	0.454	1.287
1997	1.000	4.399	0.200	0.333	0.400	0.333	0.866
1998	0.771	4.150	0.119	0.356	0.178	0.356	0.830
1999	0.659	3.243	0.152	0.456	0.152	0.405	1.013
2000	1.101	3.916	0.184	0.612	0.122	0.184	0.979
2001	1.158	4.247	0.193	0.515	0.064	0.257	0.965
2002	1.495	3.706	0.325	0.650	0.064	0.325	1.300
2003	1.545	3.477	0.258	0.837	0.064	0.322	1.416

190

191 Note: Values extracted from Rand Report. K. Symthe.: Trends in SF₆ Sales and End-Use
192 Applications: 1961-2003. Rand Corporation. 3rd International Conf. on SF₆ and the
193 Environment 1-2 December 2004.194 *Assumes worse case that sales=consumption=emission with Magnesium, Electronics and
195 other uses all being prompt releases.

196

197 Table S3. InTEM emissions estimates for South Korea.

198

Year	South Korea (t)	Uncertainty (t)
2007	190	(170-210)
2008	230	(210-250)
2009	280	(260-300)
2010	250	(230-260)
2011	190	(170-200)
2012	210	(190-220)
2013	240	(220-250)
2014	300	(280-320)
2015	350	(330-370)
2016	310	(280-330)
2017	300	(280-320)
2018	280	(260-300)

199 Average 260 (0.26Gg) (240-280)